Optimization of homogenization cycles for Ni-based superalloys

Grant Hinkle, Sam Humphrey, Adam Miller, Eric Rohrbach
Faculty Advisors: Michael Titus
Industrial Sponsors: Rob Christiansen
PURDUE MATERIALS ENGINEERING

New homogenization cycles for HASTELLOY® X alloy Ni-22Cr-18-Fe-9Mo and HAYNES® 263 alloy Ni-20Co-20Cr-6Mo (wt%) were designed to reduce energy consumption during processing in order to maintain ISO 50001 accreditation. Thermodynamic modeling was used to estimate incipient melting points, which provided a starting point for experimental trials. These experiments yielded optimal temperature and hold steps for the proposed heating cycle. This cycle reduced the hold time by 37.5% while maintaining or exceeding the current homogenization expectation. Degree of homogeneity was determined by measuring area percent of carbides.

This work is sponsored by Haynes International, Kokomo, IN

Project Background

Haynes International is a manufacturer of nickel-based superalloys mainly used in aerospace and chemical processing applications. The processing of these alloys is laid out in Figure 1.

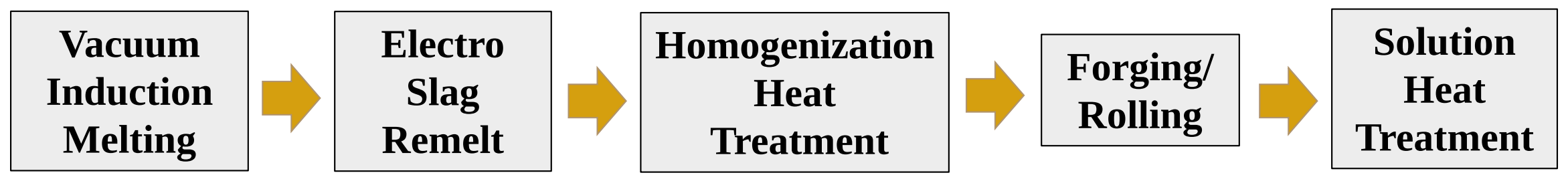
Vacuum Induction Melting → Electro Slag Remelt → Homogenization Heat Treatment → Forging/ Rolling → Solution Heat Treatment

Figure 1: Superalloy processing steps.

During casting, Nickel-based superalloys exhibit wide freezing ranges, which result in large degrees of microsegregation. This necessitates the use of homogenization heat treatments in order to redistribute alloying elements and dissolve secondary phases that form in interdendritic regions.

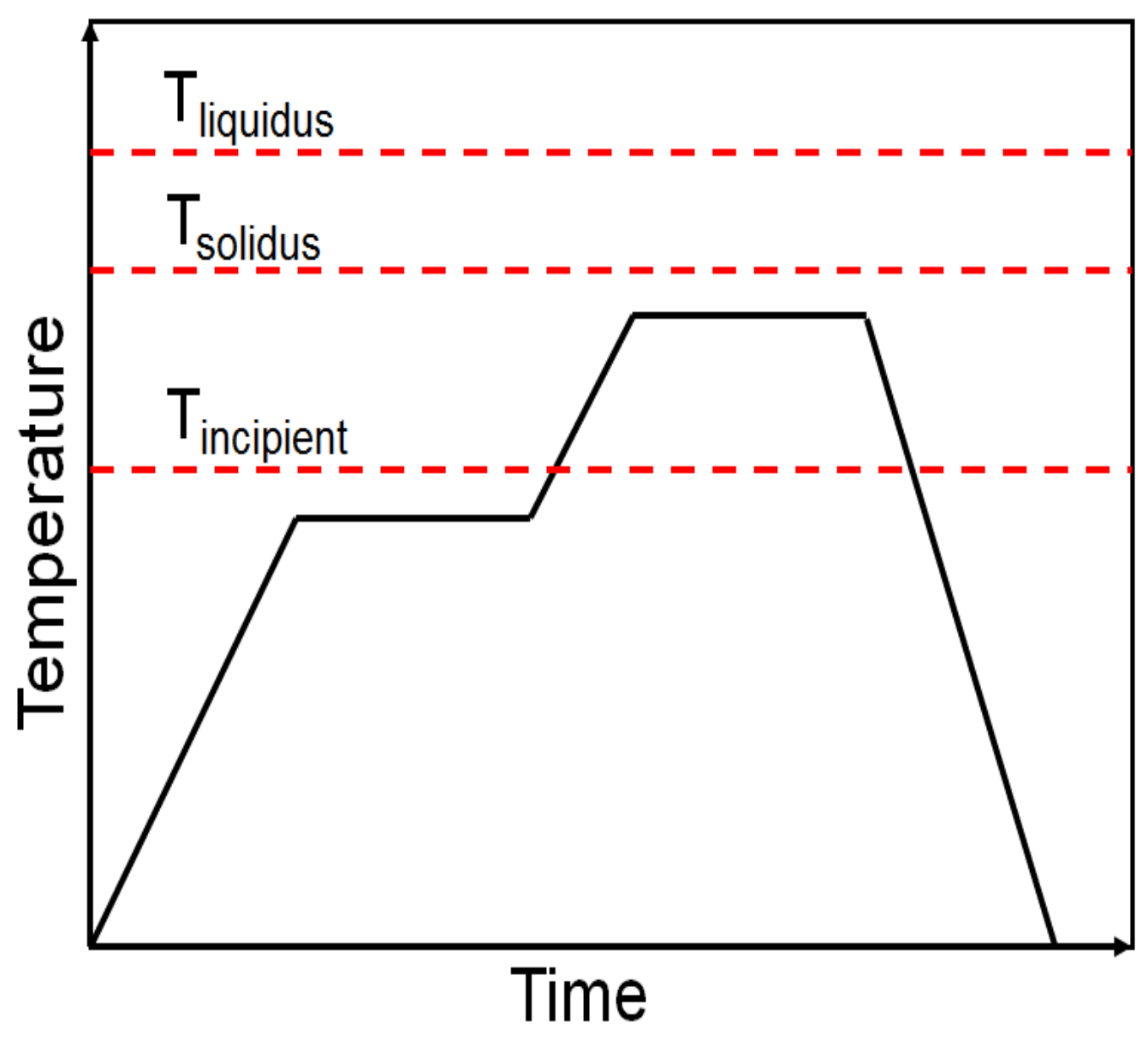

Figure 2: Schematic of optimized homogenization cycle.

The hotter the material, the more quickly diffusion occurs, carbides dissolve, and the alloy is homogenized.[1] Carbide dissolution is limited by solute diffusion into the matrix away from the carbide interface, following Fick's Law, $J = -D\frac{dc}{dx}$.[2]

Incipient melting, which occurs in localized regions of lower solidus temperatures, is detrimental to the alloy's properties. During heat treating, secondary phases dissolve and the incipient melting temperature approaches the equilibrium solidus temperature (Figure 2).[3]

As-cast Structures and Carbide Chemistry

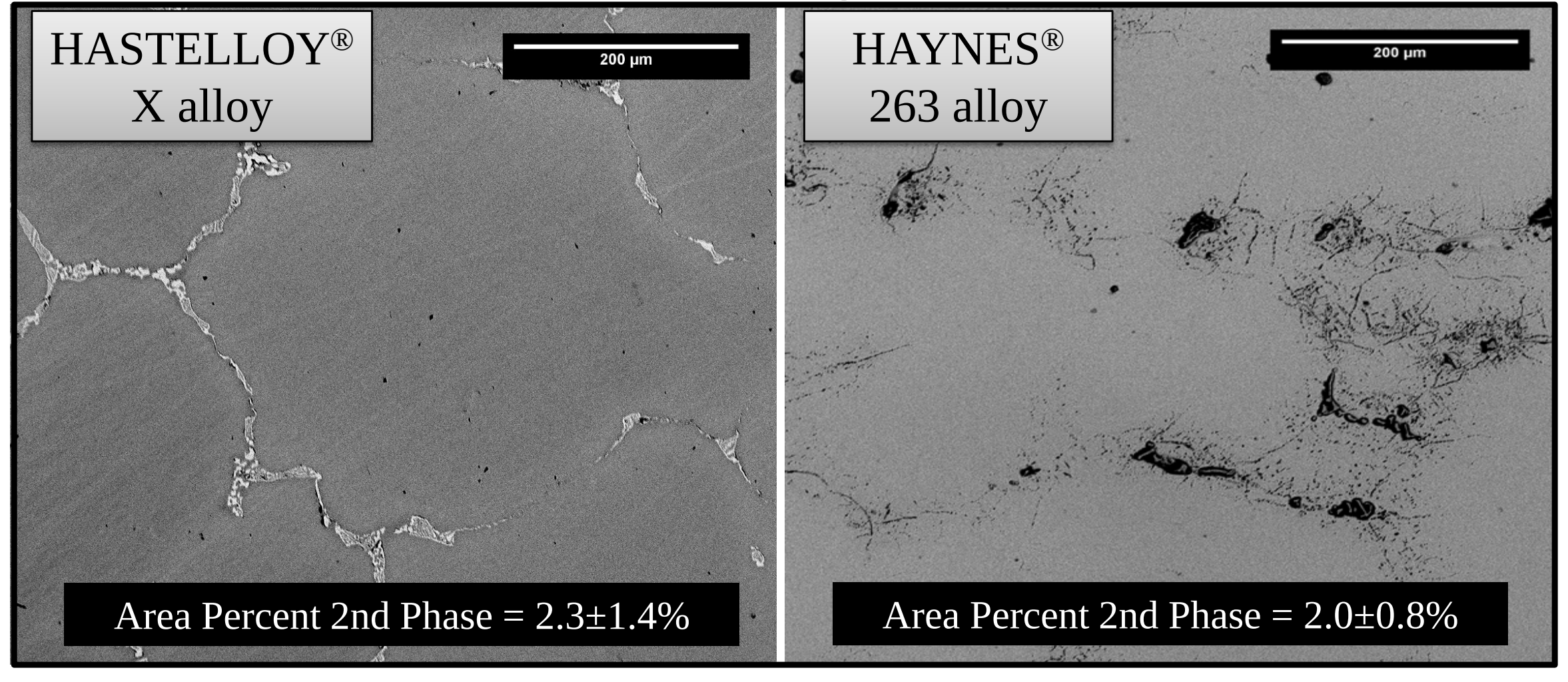

Figure 3: As-cast structures of HASTELLOY® X alloy with 2.3% area of second phases and HAYNES® 263 alloy with 2.0% area of second phase, measured on a 95% confidence interval.

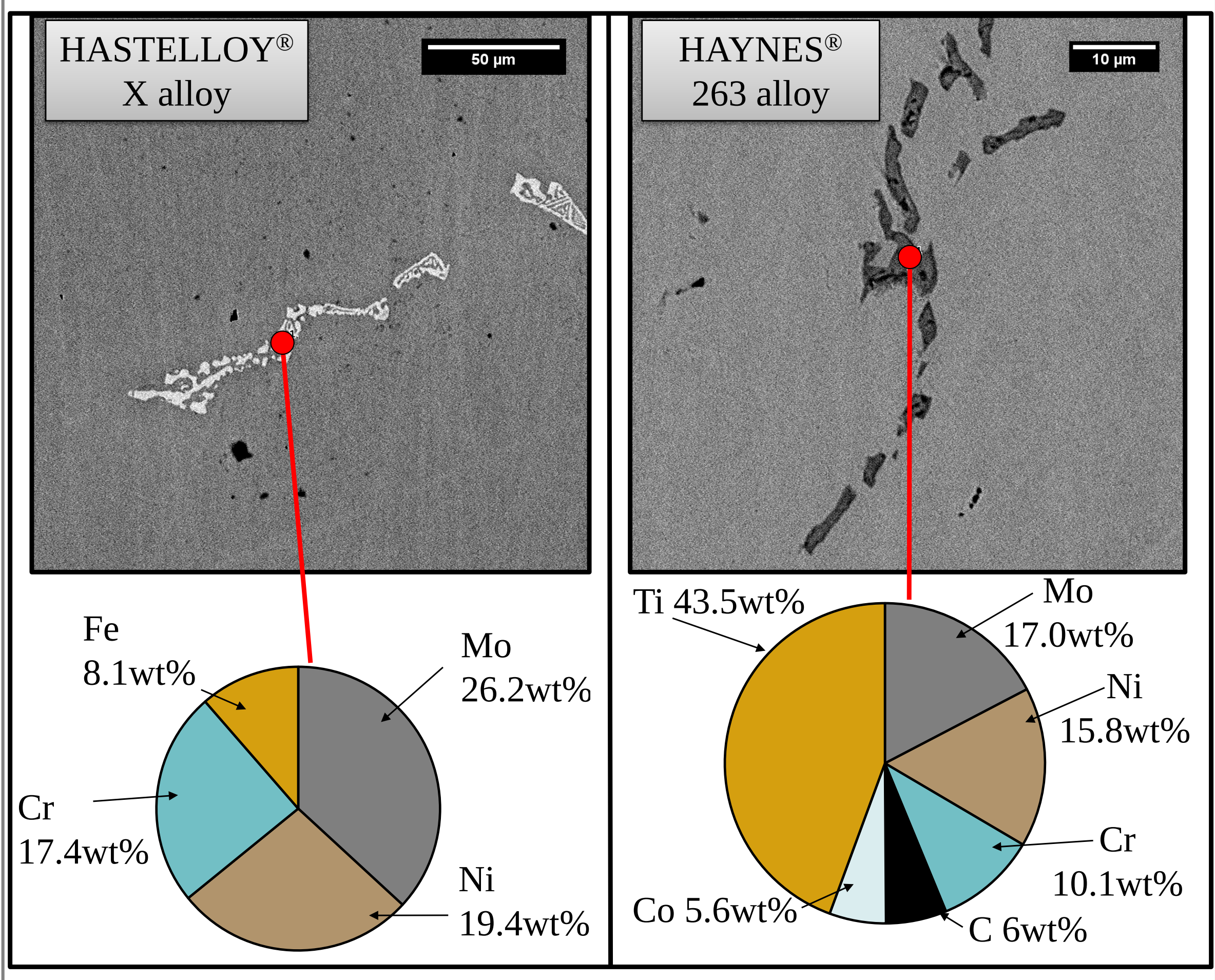

Figure 4: EDS point scans with pie charts indicating compositions for carbides present in HASTELLOY® X alloy and HAYNES® 263 alloy.

Thermodynamic Modeling for Phase Identification and Carbide Morphology

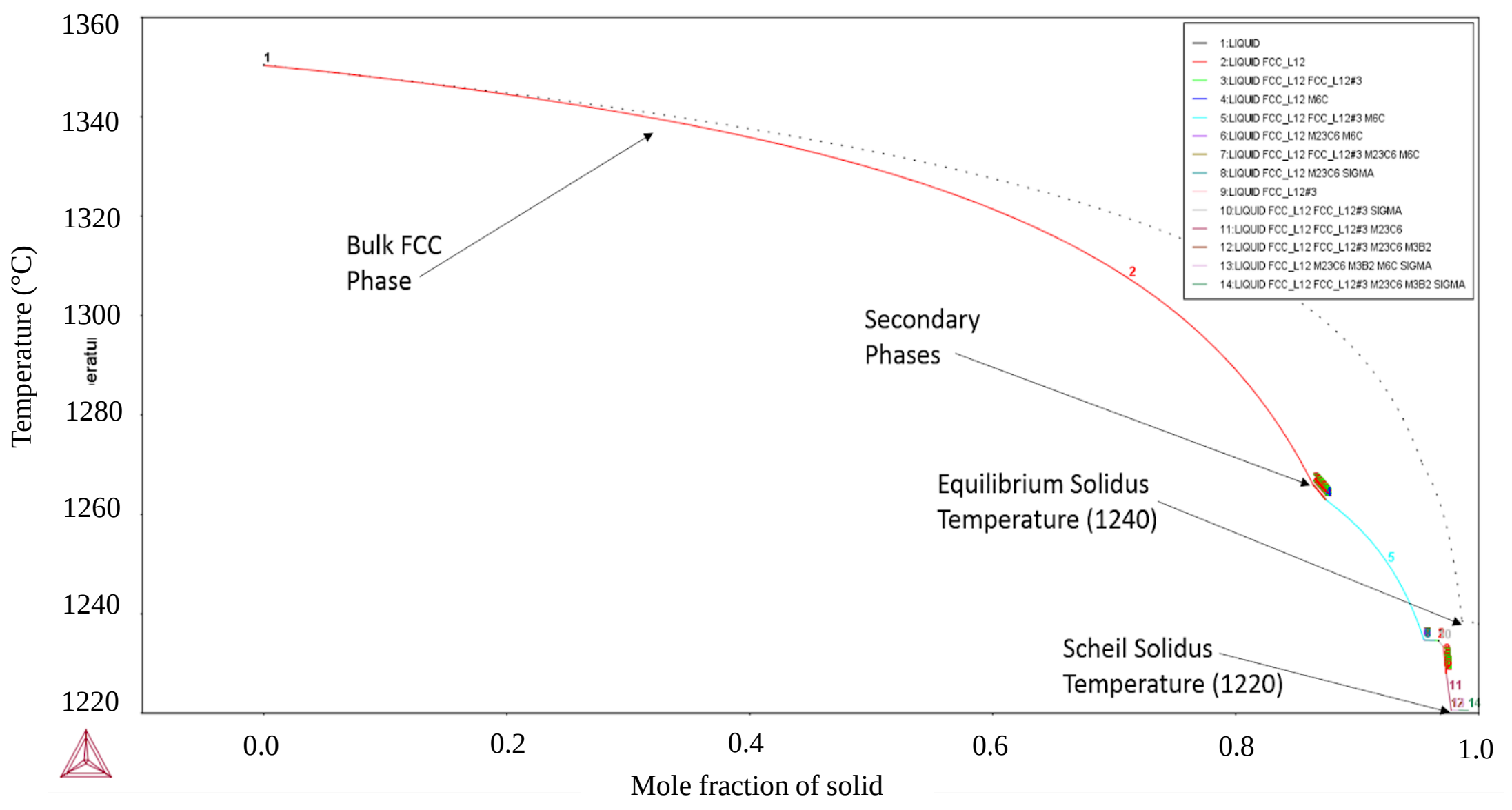

Figure 5: Scheil curve for HASTELLOY® X alloy used to determine Scheil solidus (incipient melting temperature), equilibrium solidus temperatures, and to identify phases present.

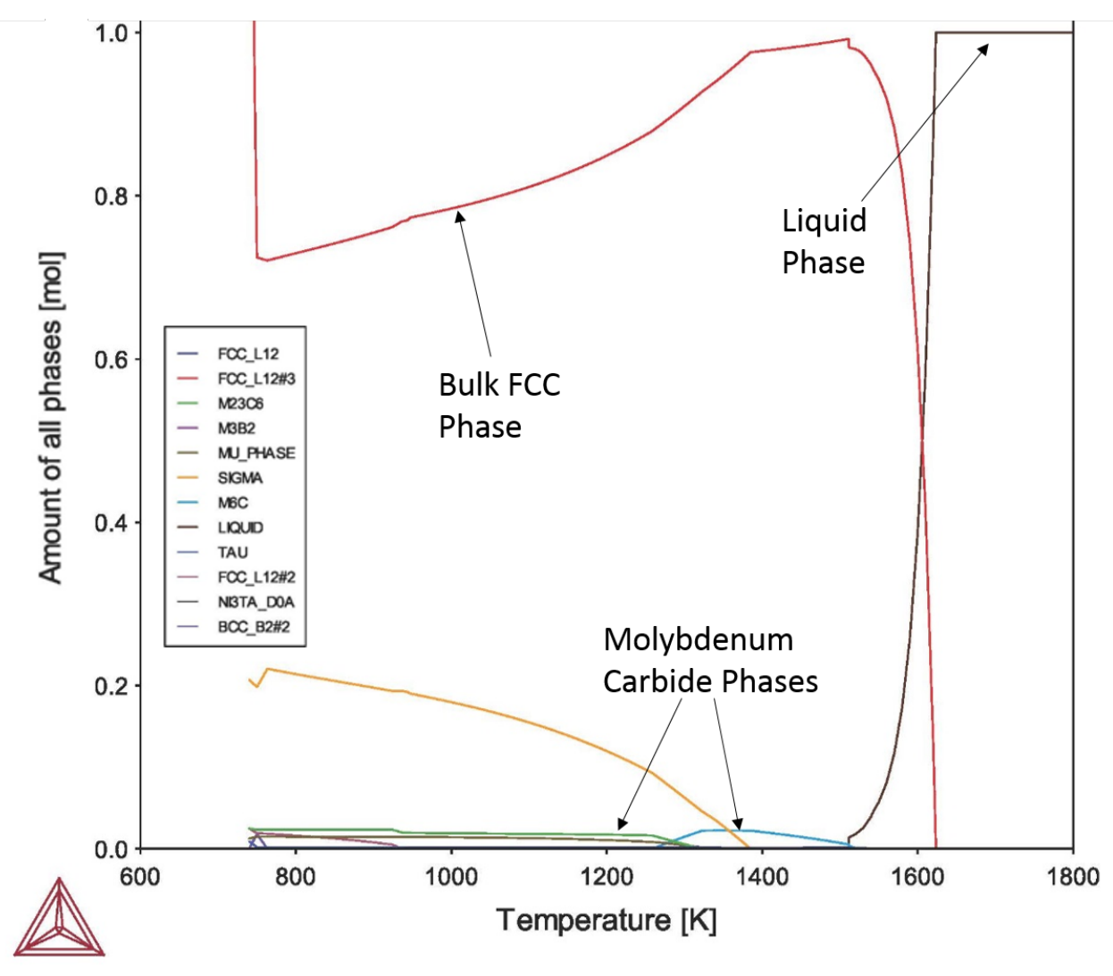

Figure 6: Equilibrium phase fractions present over relevant heat treatment ranges in HASTELLOY® X alloy.

Thermodynamic modeling suggested that the incipient melting temperatures for HAYNES® 263 alloy and HASTELLOY® X alloy are 1210°C and 1220°C, respectively (Figure 5). According to equilibrium data, $M_{23}C_6$ and M_6C are the most significant secondary phases (Figure 6).

Results – Incipient Melting

Thermodynamic modeling data was used to design experimental trials in order to experimentally determine the as-cast Scheil temperatures (Table 1).

Table 1: Experimental trials used to establish initial hold temperature.

Cycle	Incipient melting?
1200°C, 2 hrs	Yes
1190°C, 3 hrs; 1220°C, 2 hrs	Yes
1180°C, 3 hrs; 1220°C, 2 hrs	No
1180°C, 2 hrs; 1220°C, 2 hrs	Yes

Incipient melting indicated that the alloy got too hot too quickly. Therefore, more time was needed at lower temperatures to homogenize the material and to push up the Scheil temperature. Experimentally, the incipient melting temperature was found to be around 1190°C for both alloys (Table 1).

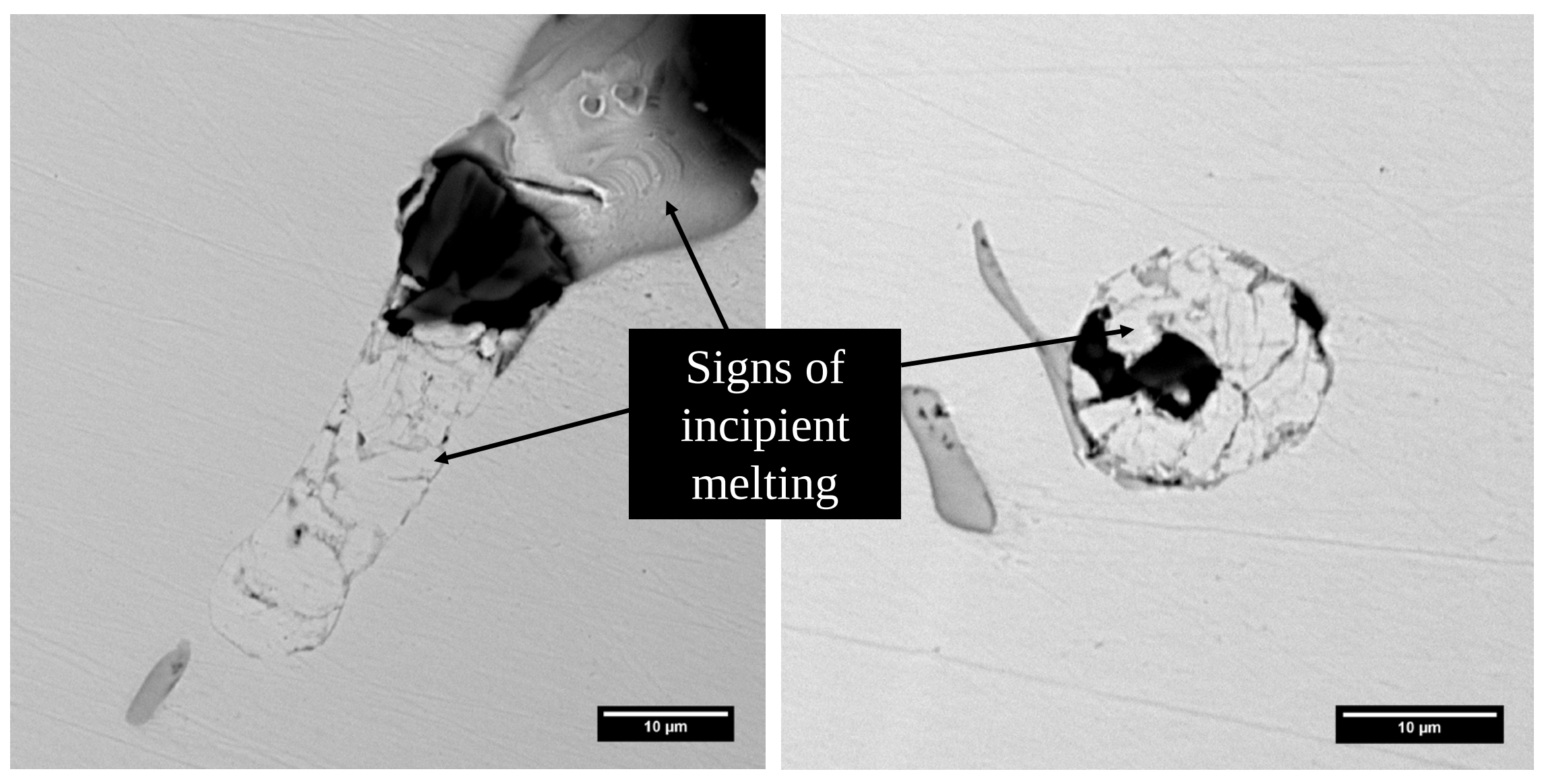

Figure 7: SEM micrographs showing incipient melting that occurred during experimental trials

Results and Discussion

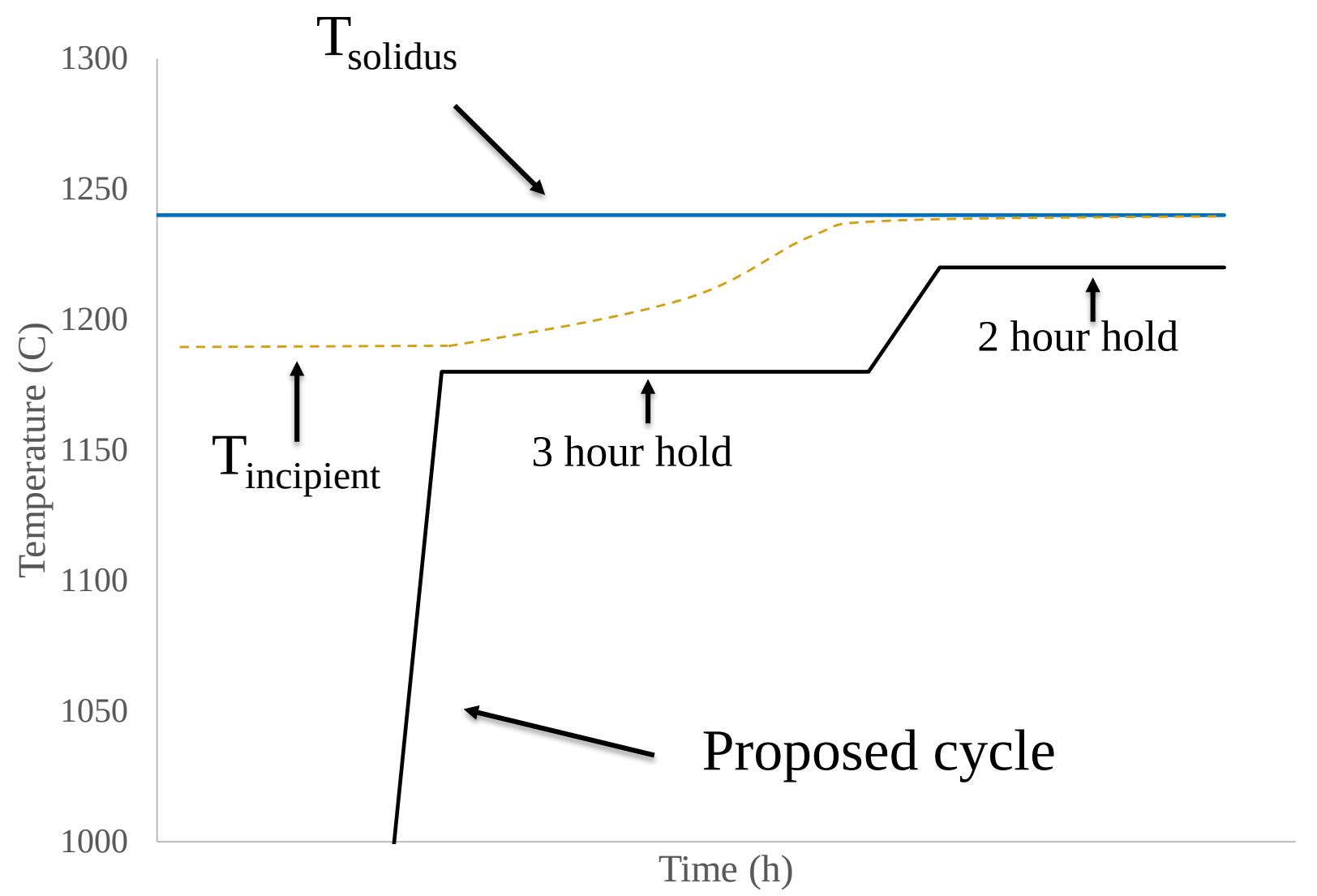

Figure 8: Proposed cycles for HAYNES® 263 alloy and HASTELLOY® X alloy.

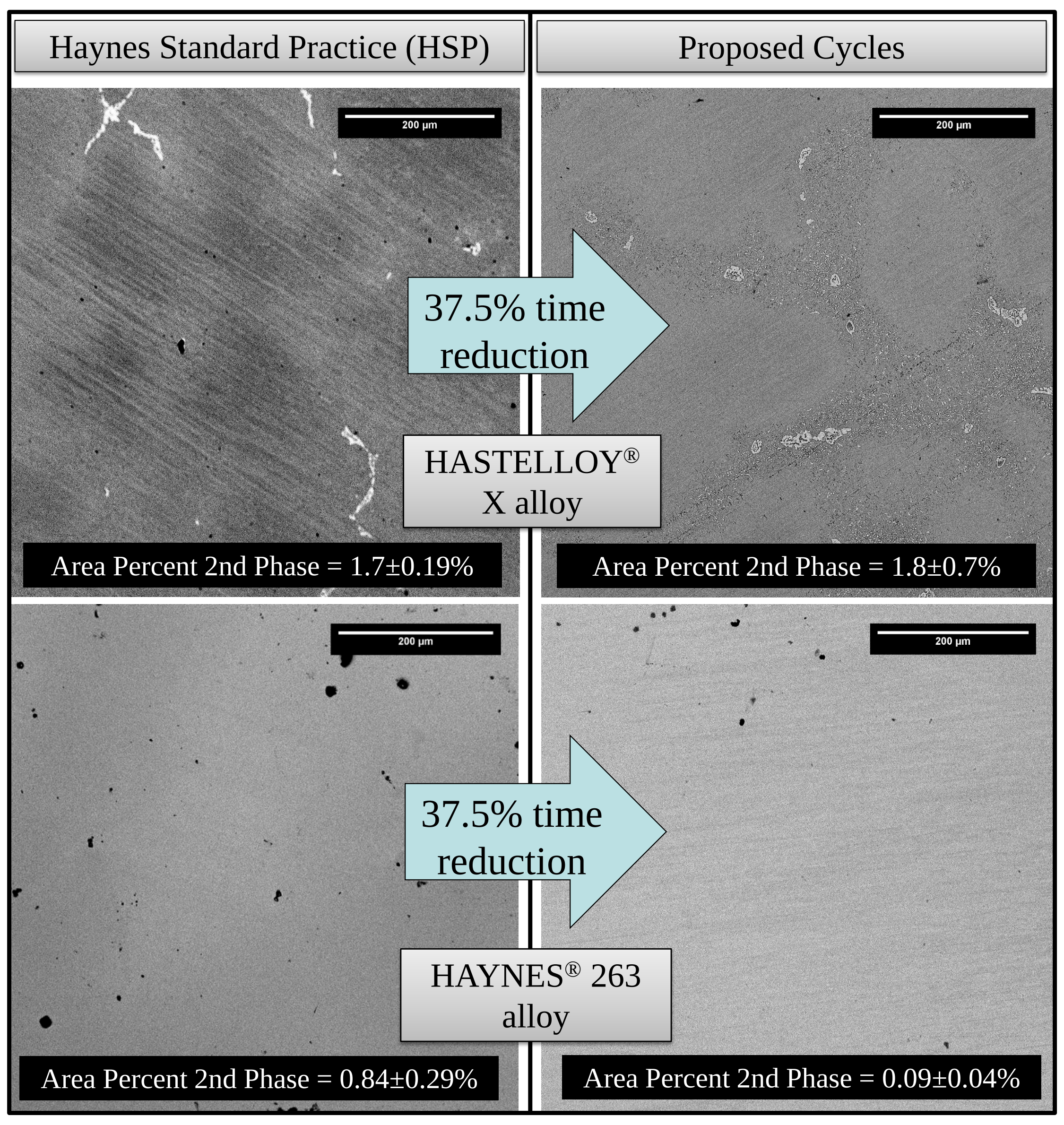

Figure 9: Microstructural comparison of HSP and proposed cycles for HASTELLOY® X alloy and HAYNES® 263 alloy with area percent second phase measured on a 95% confidence interval.

The proposed cycle for both alloys yielded reductions in area fraction of second phases similar to or exceeding HSP (Figure 9). Additionally, the hold times were reduced by 37.5%. There was a larger compositional difference between the Ti-rich carbides and the HAYNES® 263 alloy matrix compared to that of the Mo-rich carbides and the HASTELLOY® X alloy matrix (Figure 4). Because of this, HAYNES® 263 alloy experienced a steeper compositional gradient, and the solutes experienced a greater diffusional flux, increasing the rate of carbide dissolution (Equation 1). This could explain why the homogenization of HAYNES® 263 alloy exceeded HSP and the homogenization of HASTELLOY® X alloy did not.

Recommendations

- Develop a carbide dissolution curve by varying the final hold time to determine specific recipes for target carbide area fractions (Figure 10).
- Investigate how carbide morphology affects dissolution rate.

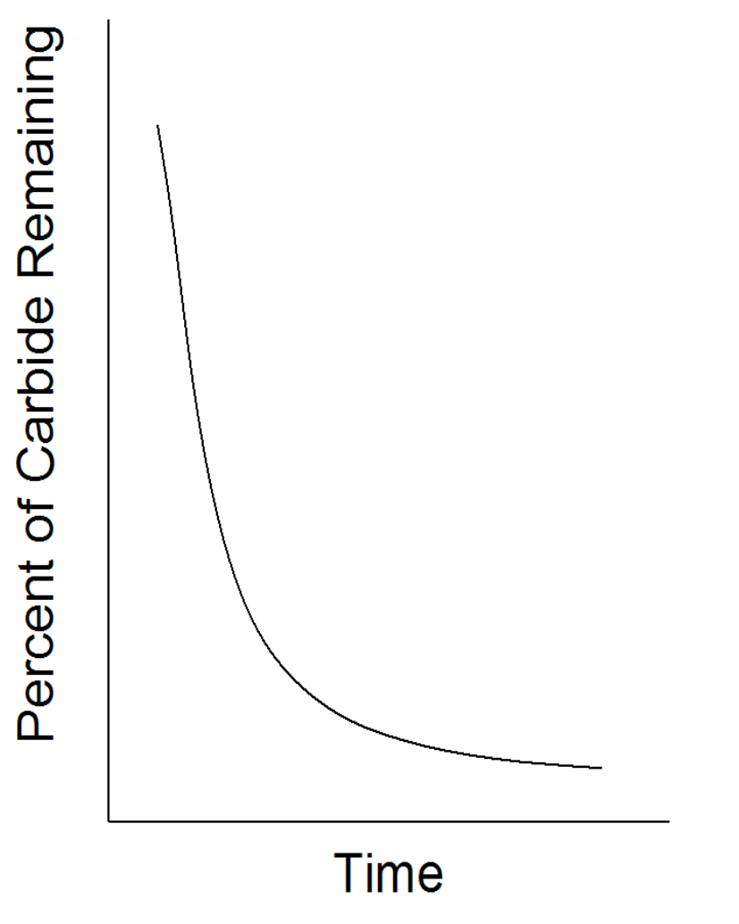

Figure 10: General carbide reduction curve.

References

1. P.D. Jablonski, C.J. Cowen, "Homogenizing a Nickel-Based Superalloy: Thermodynamic and Kinetic Simulation and Experimental Results", The Minerals, Metals, & Materials Society and ASM International, (2009) 184 vol 40B.28
2. Xu, M. L. (2012). Secondary Carbide Dissolution and Coarsening in 13% Martensitic Stainless Steel During Austenitizing (Doctoral dissertation).
3. Mostafavi, E. & Ataie, A. (2015). Destructive Interactions between Pore Forming Agents and Matrix Phase during the Fabrication Process of Porous BiFeO3 Ceramics. Journal of Materials Science and Technology -Shenyang-

MSE 430-440: Materials Processing and Design